Theor Chem Acc (2001) 106:10–21
DOI 10.1007/s002140000226

Theoretical
Chemistry Accounts

Regular article

Influence of ligand binding on the conformation of *Torpedo californica* acetylcholinesterase

Nathalie Boutonnet[1], **Daniel Van Belle**[2], **Shoshana J. Wodak**[3]

[1]Ingénierie Biomoléculaire, CP 165/64, 50 av. F. Roosevelt, 1050 Brussels, Belgium
[2]Unit of Bioinformatics, CP300, Rue Jeener & Brachet, 12, 6041 Gosselies, Belgium
[3]Université Libre de Bruxelles, U.C.M.B, CP 160/16, 50 av. F. Roosevelt, 1050 Brussels, Belgium

Received: 21 July 2000 / Accepted: 18 September 2000 / Published online: 28 February 2001

Abstract. With the aim of identifying structural changes in acetylcholinesterase, induced by ligand binding, we use a completely automatic procedure to analyse the differences between the backbone conformation of the free enzyme and those in eight complexes of *Torpedo californica* acetylcholinesterase, with various quaternary ammonium ligands, and with the protein inhibitor fasciculin. In order to discriminate between structural changes due to ligand binding and those arising from model imprecision, we also examine protein–ligand and protein–water contacts. Except for the peptide flip in the complex with huperzine A, the backbones of other complexes with quaternary ammonium ligands display negligible changes relative to the free enzyme. Another exception is the complex with the bisquaternary ammonium ligand decamethonium, where several loops display above average deformations, but only two, those spanning residues 334–348 and residues 277–304, seem to move as a result of ligand binding. Movement of the ω loop (residues 61–95) is detected only in the complex with the protein fasciculin.

Key words: Structural changes – Acetylcholinesterase – Structure alignment program

1 Introduction

The enzyme acetylcholinesterase (AChE) terminates nerve impulse transmission at cholinergic synapses by rapid hydrolysis of the neurotransmitter acetylcholine into choline and acetic acid [1]. Understanding at the atomic level the mechanism whereby various ligands inhibit this enzyme should be of help in designing new therapeutic agents in diseases such as Alzheimer's disease [2] that involve acetylcholine insufficiencies.

The apparent complexity of AChE inhibition resides primarily in the features of the enzyme 3D structure [3], as revealed by the crystal structure of *Torpedo californica* AChE (TcAChE) [4] and confirmed by those of variants from other organisms [5, 6]. The active-site triad (S200, E327, H440) is located at the bottom of a long and narrow gorge, whose lining is composed of 40% of aromatic side chains. The bottom of the gorge features an "esteratic" subsite, containing the catalytic apparatus, and a separate "anionic" subsite, which binds the quaternary group of the substrate [7]. Various studies also support the existence of a second "peripheral" anionic site, 14 Å from the first, closer to the top of the gorge [8, 9]. According to the type of ligand occupying this site, the enzyme can be either activated or inhibited. Alternatively, the site can serve as an intermediate halt for ligands travelling towards the active pocket [10].

A number of crystallographic studies have been devoted to the analysis of AChE–ligand complexes. They illustrate well the diversity and complexity of the underlying interactions. The complexes studied involve inhibitors as chemically diverse as decamethonium (DEC), edrophonium (EDR), tetrahydroaminoacridine [11], *m*-(*N*,*N*,*N*-trimethylammonio)trifluoroacetophenone (TMTFA) [10], (-)-huperzine A (HUP) [12], polyacrylamide (PAM) and (*R*,*S*)-1-benzyl-4-[(5,6-dimethoxy-1-indanon)2-yl]methylpiperidine (E2020) [13] as well as a protein inhibitor, the snake toxin fasciculin (FAS) [14]. In these complexes some of the inhibitors are found to bind in or near the anionic and esteratic active site pockets, whereas others interact more exclusively with the peripheral site. Some bisquartenary cations, such as DEC, are shown to span both sites, a likely reason for their enhanced potency relative to monoquaternary ligands. Many of the ligands analysed are rather bulky, suggesting that the enzyme must display appreciable flexibility to allow them to penetrate the deep gorge and bind to the observed sites. The short time scale of the TcAChE enzymatic reaction [15] suggests that this must involve negligible energy barriers. Identifying the regions

Correspondence to: N. Boutonnet

Contribution to the Symposium Proceedings of Computational Biophysics 2000

of the enzyme undergoing movement upon ligand binding has, therefore, been of interest.

The comparison of the complexed and free enzyme crystal structures revealed only very minor differences in the backbone conformations, ranging between 0.3 and 0.4 Å root mean square (rms) [11, 13]. Also, with hardly any detectable backbone changes, these studies focused mainly on commenting reorientation of key side chains such as Phe_{330} and Trp_{279} or changes in the pattern of interactions with water molecules [13]. Small changes in the backbone of several loops were also reported for the complex of TcAChE with FAS [14].

Here we report a systematic analysis of the differences in the backbone structures between a large number of available complexed forms of TcAChE, including those with quaternary ligands and the protein FAS, and the corresponding ligand-free enzyme solved at 2.5 Å (2ACE). To this end we use a completely automatic procedure for analysing structural changes in two proteins developed by some of us [16]. This procedure was shown to describe conformational changes in a variety of systems and that even in cases where the structural changes were very limited. It therefore seemed appropriate to use it in order to identify ligand-induced structural changes in the AChE system. However, in addition to the small magnitude of the expected structural changes, the AChE system presents a major difficulty. The atomic models available for most of the complexes have been derived from 2.8–3.0-Å resolution electron density maps before the R-free based refinement became common practice, and are hence not of the highest quality. Thus, a major challenge facing an analysis such as that proposed here is the ability to distinguish amongst the identified structural changes, those caused by ligand binding from those arising from model imprecisions.

To meet this challenge, we first analyse the changes in the three higher-quality structures of the HUP–TcAChE, E2020–TcAChE and EDR–TcAChE complexes, solved at 2.5 and 2.4 Å resolution, respectively. Then the changes identified in these complexes and those detected in the less accurate structures (2.8 Å) of the other TcAChE complexes are compared. Our automatic procedure is used to derive optimal global structure superpositions of the complexes relative to the free enzyme. In addition, it identifies the protein segments that undergo local deformation as well as groups of segments which move as rigid bodies. These analyses are performed for the different complexes, and their relevance to ligand binding is validated by analysing protein contacts with the ligands and with crystallographic solvent molecules.

This yields a consistent picture, which provides useful insight into how the ligands considered may influence the conformation of TcAChE in the crystal. It also illustrates some of the limitations encountered in extracting information on structural flexibility from crystallographic data.

2 Methods

2.1 Structural similarities between two polypeptide chains

The comparison between the 3D structures of two polypeptide chains was performed using the structure alignment program SoFi [17]. This algorithm uses as sole structural similarity to measure the rms deviation (rmsd) of N, Cα, C and O backbone atoms after coordinate superposition and is designed to determine the best match between all short segments of the two chains yielding the lowest global rmsd. To this end, the procedure first identifies all overlapping segments of a given length with similar backbone conformations in both 3D structures. Conformational similarity is evaluated by the rmsd value. Next, to obtain the global alignment of the two proteins, the pairs of equivalent segments are assembled, in order of decreasing structural similarity, by a multiple-linkage hierarchic clustering algorithm (MLC). This algorithm generates several intertwined clustering trees. From these trees, solutions corresponding to the best alignments are selected. In a final stage, the aligned segments are extended at both ends to include residues outside the initial segment limits.

2.2 Analysing conformational changes between different 3D structures of the same protein

The conformational changes between two different 3D structures of the same protein are detected using a fully automatic procedure [16]. This procedure uses as its sole information the atomic coordinates of the structures and involves two main steps, which can be summarized as follows.

The first step of this method is a variant of the procedure described in the previous section. It operates by first deriving the global 3D structure alignment between the two proteins using a MLC procedure. Since the limits of secondary structures tend to be the same in the two protein structures to be compared, the equivalent chain segments that we cluster correspond to the secondary structure elements (α helices and β strands) and/or loops (defined as all regions outside the secondary structures). The limits of these segments are determined by the DSSP algorithm [18].

In the second step, the resulting intertwined clustering trees are analysed in order to extract information on the rigid static core, defined here as the secondary structure elements, which do not move in the conformational change, and on the movers (segments of secondary structure and loops), whose conformation or spatial positions relative to the static core differs in the two structures. For that purpose, the intertwined trees are automatically scanned to determine the jump-minimizing path. By construction, this path groups the structural elements which move least in the conformational change. It starts at the node with lowest rmsd and travels down the trees through successive nodes, such that when moving from one node to the next, the difference in the rmsd is a minimum. The static core is defined as the node along this path which is separated by a large enough rmsd change from the following node. Once the static core is identified, the remaining fragments, which are added onto it along the jump-minimizing path define the principal movers. The size of the rmsd jump, produced when they are assembled, determines their category as minor or major movers.

3 Results

3.1 Structural changes induced by ligand binding

In the following we present the results obtained with our automatic procedure on the structural changes observed in seven complexes of TcAChE with quaternary ammonium ligands, EDR (PDB code 2ACK), tacrine (PDB code 1ACJ), DEC (PDB code 1ACL) as well as with other ligands, PAM, TMTFA (PDB code 1AMN), HUP (PDB code 1VOT) and E2020 (PDB code 1EVE). The structural changes are analysed relative to the structure of the free enzyme determined at 2.5-Å resolution (PDB code 2ACE). Throughout the remaining sections, all the structures analysed are referred to by their PDB codes or by the abbreviated ligand names. An annotated ribbon drawing of this TcAChE structure is presented in Fig. 1.

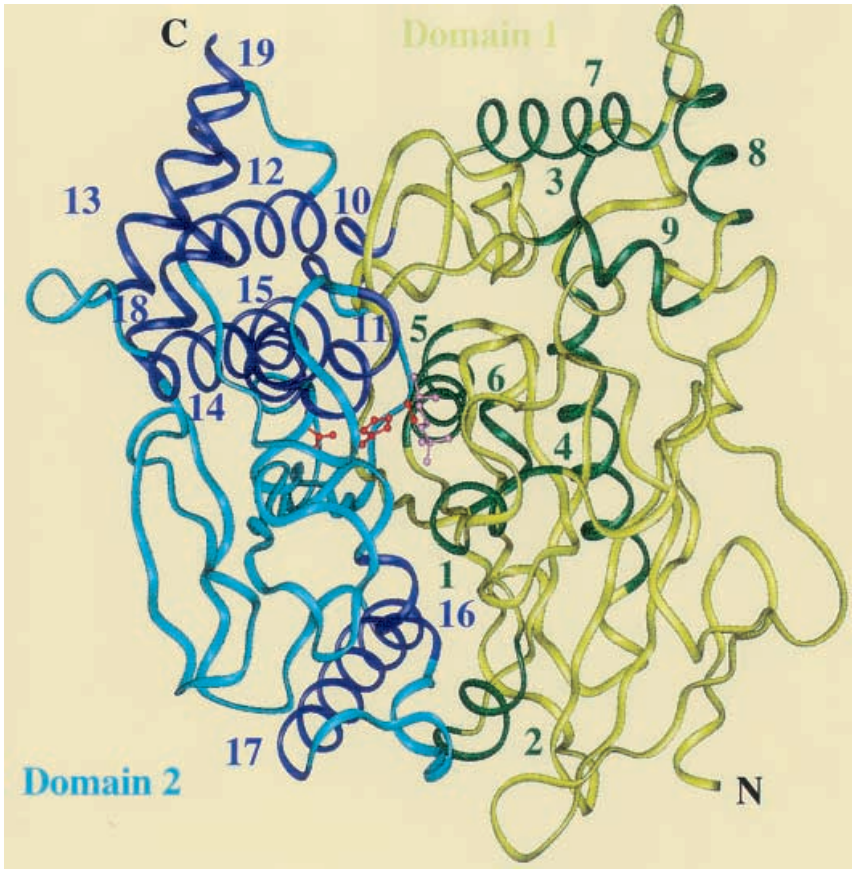

Fig. 1. Ribbon diagram of the crystal structure of *Torpedo californica* acetylcholinesterase (*TcAChE*) (PDB code 2ACE). Residues 4–305 are coloured *green* and residues 306–535 are coloured *cyan*, highlighting the two domains of the molecule as defined in Ref. [19]. The *dark-labelled* segments correspond to α helices. Side chains of the catalytic triad (Ser_{200}, His_{440}, Glu_{327}) are shown in *red stick* form. The choline molecule is displayed in *pink*. The N and C termini are marked. This figure was generated using the InsightII software

This figure also highlights the two structural domains of AChE, as defined in Ref. [19].

3.1.1 Global structural comparisons

The backbone rmsds obtained by the MLC procedure for the global alignments between each of the structures analysed and the free enzyme 2ACE are listed in Table 1. The rmsd values range between 0.18 and 0.36 Å for the secondary structures and between 0.20 and 0.43 Å when the loop regions are included. Our automatic analysis hence confirms earlier observations [11,13] that the presence of various inhibitors in the crystal structure of TcAChE causes extremely small changes in the overall conformation of the protein. In particular, the changes between the free enzyme and the two complexed structures 1VOT and 2ACK, determined at higher resolution, are virtually negligible (less than 0.22 Å). We see nevertheless that the rmsds computed considering both secondary structure elements and loop regions are systematically higher by about 0.02–0.08 Å than those computed considering only secondary structures.

In what follows we describe how the detailed analysis of the local structural deformations and rigid-body movements, performed with the MLC procedure, is nonetheless capable of identifying in some of the complexes considered, a small subset of local deformations, mainly in loop regions, which may be linked to ligand binding.

Table 1. Backbone root mean square deviations (*rmsds*) for the global structure alignments between the free *Torpedo californica* acetylcholinesterase (*TcAChE*) (PDB code 2ACE) and its ligated structures. The name of the ligand and the PDB code of each complex being compared to 2ACE are listed in column 1. The resolution of the whole structure is indicated in column 2. The rmsds (in angstroms) between the superimposed backbones of all the secondary structures in the two forms are listed in column 3. The rmsd of the whole structure is given for each pairwise alignment in column 4

Complex	Resolution (Å)	Backbone of secondary structures rmsd (Å)	Entire backbone rmsd (Å)
HUP (1VOT)	2.5	0.18	0.20
EDR (2ACK)	2.4	0.18	0.22
E2020 (1EVE)	2.5	0.28	0.33
DEC (1ACL)	2.8	0.35	0.43
PAM	2.8	0.36	0.41
THA (1ACJ)	2.8	0.33	0.39
TMTFA (1AMN)	2.8	0.35	0.41
FAS (1FSS)	3.0	0.43	0.51

3.1.2 Local structural changes

The backbone rmsds for individual pairs of secondary structures and loops in the various complexes versus those in the free enzyme are listed in Tables 2 and 3. The rmsd values for the higher resolution structures are listed in Table 2, while those for the lower resolution one are listed in Table 3. In Table 3, we list only segments with rmsd of values of 0.4 Å or greater.

Table 2. Deformations of individual secondary structures and loops in the complexes of TcAChE with the ligands HUP, EDR and E2020. Column 1 lists the secondary structure elements and loops numbered according to the order in which they occur in the polypeptide chain. Their limits, defined in the free enzyme 2ACE according to DSSP [18], are indicated in column 2. Columns 3–5 list the rmsds (in angstroms) between the superimposed backbones of the 2ACE and those of the HUP–TcAChE, EDR–TcAChE and E2020–TcAChE complexes. The α17-β13 loop is divided into two parts because some residues in the middle of the loop have missing atomic coordinates. Values in *bold* correspond to rmsd of 0.4 Å or greater

Domain 1				
		HUP 1VOT	E2020 1EVE	EDR 2ACK
β1	7–10	0.15	0.27	0.12
β1-β2	11–12	0.04	0.11	0.09
β2	13–16	0.12	0.16	0.11
β3	18–21	0.19	0.24	0.21
β3-β4	22–25	0.30	**0.55**	**0.91**
β4	26–34	0.13	0.29	0.15
β4-β5	35–56	0.16	0.25	0.20
β5	57–59	0.16	0.23	0.21
β5-α1	60–78	0.17	0.30	0.18
α1	79–82	0.11	0.16	0.11
α1-β6	83–95	0.12	0.20	0.17
β6	96–101	0.13	0.16	0.08
β6-β7	102–108	0.19	0.24	0.19
β7	109–115	0.14	0.21	0.12
β7-α2	116–132	**0.50**	0.18	0.19
α2	133–139	0.11	0.21	0.17
α2-β8	140–141	0.10	0.09	0.05
β8	142–145	0.13	0.14	0.12
β8-α3	146–151	0.09	0.16	0.11
α3	152–155	0.13	0.16	0.16
α3-α4	156–167	0.18	0.31	0.18
α4	168–183	0.14	0.18	0.17
α4-β9	184–188	0.13	0.23	0.15
β9	189–199	0.14	0.23	0.15
α5	201–209	0.14	0.14	0.11
α5-α6	210–212	0.12	0.18	0.09
α6	213–216	0.12	0.22	0.11
α6-β10	217–220	0.12	0.13	0.11
β10	221–225	0.10	0.14	0.09
β10-α7	226–237	0.13	0.18	0.16
α7	238–250	0.18	0.17	0.15
α7-α8	251–258	0.17	0.29	0.14
α8	259–268	0.18	0.24	0.13
α8-α9	269–270	0.13	0.07	0.09
α9	271–276	0.14	0.12	0.11
α9-α10	277–304	0.15	0.23	0.17
α10	305–310	0.12	0.16	0.13
α10-β11	311–318	0.12	0.19	0.11
Domain 2				
		HUP 1VOT	E2020 1EVE	EDR 2ACK
β11-α11	325–328	0.11	0.10	0.10
α11	329–333	0.15	0.24	0.15
α11-α12	334–348	0.16	0.21	0.16
α12	349–359	0.21	0.24	0.20
α12-α13	360–364	0.14	0.31	0.12
α13	365–375	0.11	0.22	0.16
α13-α14	376–383	0.19	0.21	0.18
α14	384–399	0.16	0.16	0.12
α15	401–411	0.15	0.20	0.18
α15-β12	412–417	0.27	0.23	0.12
β12	418–423	0.08	0.17	0.10
β12-α16	424–443	0.16	0.28	0.19
α16	444–447	0.18	0.14	0.15
α16-α17	448–459	0.18	0.24	0.18
α17	460–479	0.20	0.25	0.20
α17-β13N	480–484	0.10	**0.52**	**0.49**
α17-β13C	491–500	0.19	0.29	0.16
β13	501–505	0.12	0.13	0.17
β13-β14	506–511	0.20	0.36	0.18
β14	512–514	0.08	0.11	0.13
β14-α18	515–517	0.08	0.14	0.10
α18	518–525	0.10	0.18	0.11
α19	527–533	0.10	0.21	0.14

Table 3. Largest deformations of individual secondary structures and loops in the higher-resolution complexes versus those in the free form of TcAChE (2ACE). Columns 1 and 2 list, respectively, the identifications and limits of secondary structure elements and loops for each complex analysed. Columns 3–7 give the backbone rmsds of 0.4 Å or greater in the DEC, PAM, THA, TMTFA and FAS complexes versus those in the free enzyme

		DEC 1ACL	PAM	THA 1ACJ	TMTFA 1AMN	FAS 1FSS
β3-β4	22–25	0.93	1.05	0.97	1.04	1.09
β4-β5	35–56					0.40
β5-α1	60–78					0.45
α3-α4	156–167	0.79	0.75	0.76	0.77	0.55
α7-α8	251–258	0.52				
α8	259–268	0.43				
α9-α10	277–304	0.45				0.62
α10-β11	311–318					0.41
β11-α11/α11/α11-α12	325–348					0.78
α11-α12	334–348	0.54				
α13-α14	376–383	0.44			0.57	
α17-β13$_N$	480–484	0.56	0.42	0.62		0.56
α17-β13$_C$	491–500	0.51		0.50		
β13-β14	506–511					0.57

The conformations of individual secondary structure elements are virtually the same in the ligated and free structures. Indeed the rmsd values displayed in Tables 2 and 3 range between 0.08 and 0.34 Å, with only helix α8 in the DEC complex displaying a somewhat larger value of 0.43 Å. On the other hand, some loops undergo more significant changes. Here, a clear distinction can be made according to the resolution at which the crystal structures were determined. In the higher-resolution structures, only one or two loop fragments undergo significant deformation. These are the loop segments between strand β7 and helix α2 (β7-α2) in 1VOT and those between strands β3 and β4 (β3-β4) and between helix α17 and strand β13 (α17-β13$_N$) in 2ACK and 1EVE. In the lower-resolution complexes, the largest deformations occur in the β3-β4 loop, with rmsd values ranging between 0.93 and 1.05 Å and in the α3-α4 loop, whose rmsd values range between 0.56 and 0.74 Å. Most of these complexes also display a significant deformation of the α17-β13 loop. This deformation most probably originates from the fact that this segment is broken up into two parts (α17-β13$_N$; α17-β13$_C$), flanking a stretch of six residues (485–490), which could not be positioned in the electron density map in all the structures except in 1EVE. Other

observed changes occur in the α13-α14 loop in the TMTFA and DEC structures while in the latter, three additional loops α7-α8, α9-α10, α11-α12 display above-average structural deformations, as witnessed from their backbone rmsd values (0.43–0.54 Å).

In summary, the local structural deformations of the complexed versus the free form of TcAChE are confined to a few loops, which are furthermore the same for the different complexes. A few additional loops, and helix α8 undergo changes in the complex with DEC.

The relevance of these deformations to ligand binding is analysed below.

3.1.3 Identifying relative displacements of substructures

In this section, a detailed analysis of the conformational changes is made by identifying the rigid static core and the movers. This is achieved by processing the intertwined clustering trees, which describe the hierarchy of fragment grouping. We start by discussing the results obtained for the three complexes with HUP, EDR and E2020. This is followed by a detailed account of the results for the structures of the six lower-resolution complexes.

3.1.3.1 Displacements in the 2.5-Å resolution complex with HUP. The 1D representation of the jump-minimizing path obtained for the superposition of all segments (Fig. 2a) shows that all the bars except one cluster close together at very low rmsd values. This means that the corresponding segments superimpose together with a negligible rmsd, the loop β7-α2 being the only segment to induce a significant rmsd jump when added to all the others. This segment, whose backbone displays an rmsd change of 0.5 Å (Table 2) when superimposed independently, contains the flipped peptide bond between residues Gly_{117} and Gly_{118}, identified previously [12] as the unique difference between the backbone atoms of the HUP complex and those of the native enzyme structure.

This shows that our completely automatic analysis is capable of detecting without any prior knowledge a very small and localized difference between two structures, involving essentially only a few atoms. It thus demonstrates its high level of sensitivity and indicates that it is well suited for identifying small ligand-induced conformational changes of the type that we are dealing with in this study.

3.1.3.2 Displacements in the 2.4-Å resolution complex with EDR. The 1D representation of the jump-minimizing path for the superposition of the EDR-bound structure and the free enzyme (Fig. 2b) indicates that here too the vast majority of the segments superimpose as a single entity, with negligible rmsd, except two clusters that induce rmsd jumps of some significance. One is the segment β3-β4 and the other is α17-$\beta 13_N$, located just before the previously mentioned interrupted chain segment. Both segments undergo local deformations (Table 2). They are located on the opposite side of the molecule, far from the active-site gorge. It is therefore unlikely that their deformation is caused by ligand binding. On the other hand, it is plausible that they result form the uncertainty associated with the atomic coordinates in the α17-β13 segment, which might also affect those of the nearby β3-β4 loop.

These results hence suggest that binding of the EDR molecule in the active-site cleft of TcAChE in the crystal is accompanied by no change in the backbone conformation of the protein.

3.1.3.3 Displacements in the 2.5-Å resolution complex with E2020. The wider spread of the bars across the jump-minimizing path of E2020–TcAChE (Fig. 2c) compared to that in Fig. 2a and b clearly indicates that the magnitude of the computed structural differences for E2020 is significantly larger than in HUP and EDR. These changes can be attributed to the more accurate 3D structure of E2020–TcAChE relative to the free-enzyme model 2ACE. However, there is no significant rmsd jump in the projection of the jump-minimizing path. Thus, our automatic procedure confirms that the backbone of AChE is not significantly affected by the binding of E2020. Interestingly, this inhibitor interacts with the enzyme only indirectly via solvent molecules and makes no direct contacts with either the catalytic triad or the oxyanion hole [13].

3.1.3.4 Displacements in the 2.8-Å resolution complexes. The static cores of the complexes with DEC, THA, PAM and TMTFA, defined from their respective jump-minimizing paths of secondary structures, include all the secondary structure elements of each protein. The only exception is helix α8 in DEC, which is slightly displaced relative to the static core. This displacement is, however, due to the helix being locally somewhat distorted, as seen from the data in Table 3.

The 1D representation of the jump-minimizing paths of all segments generated for all the complexes are displayed in Fig. 2d, e, f and g. The magnitude of the displacement is largest in the DEC complex, followed by those in TMTFA, PAM and then THA. In all cases, the two loops α3-α4 and β3-β4 display the largest local deformations. A few other loops display lesser though still sizable rmsd jumps. The remaining great majority of the loops display no rmsd jumps. They appear indeed to "move" together with their flanking secondary structures.

The DEC complex features the largest number of movers, which may be ascribed to the fact that this ligand spans the two anionic binding sites. The extra movers (aside from α3-α4 and β3-β4) correspond to loops α7-α8 and α11-α12, as well as to the interrupted chain segments between α17 and β13.

A first obvious conclusion to be drawn from these results is that the movers are all loop segments. This is consistent with our findings that larger rmsd values were obtained for the global superpositions when the loops were included in the analysis, and is consistent with the fact that the largest local distortions occur in loop regions (Table 3).

It is important to note at this point that our analysis detects no significant structural changes in the ω loop

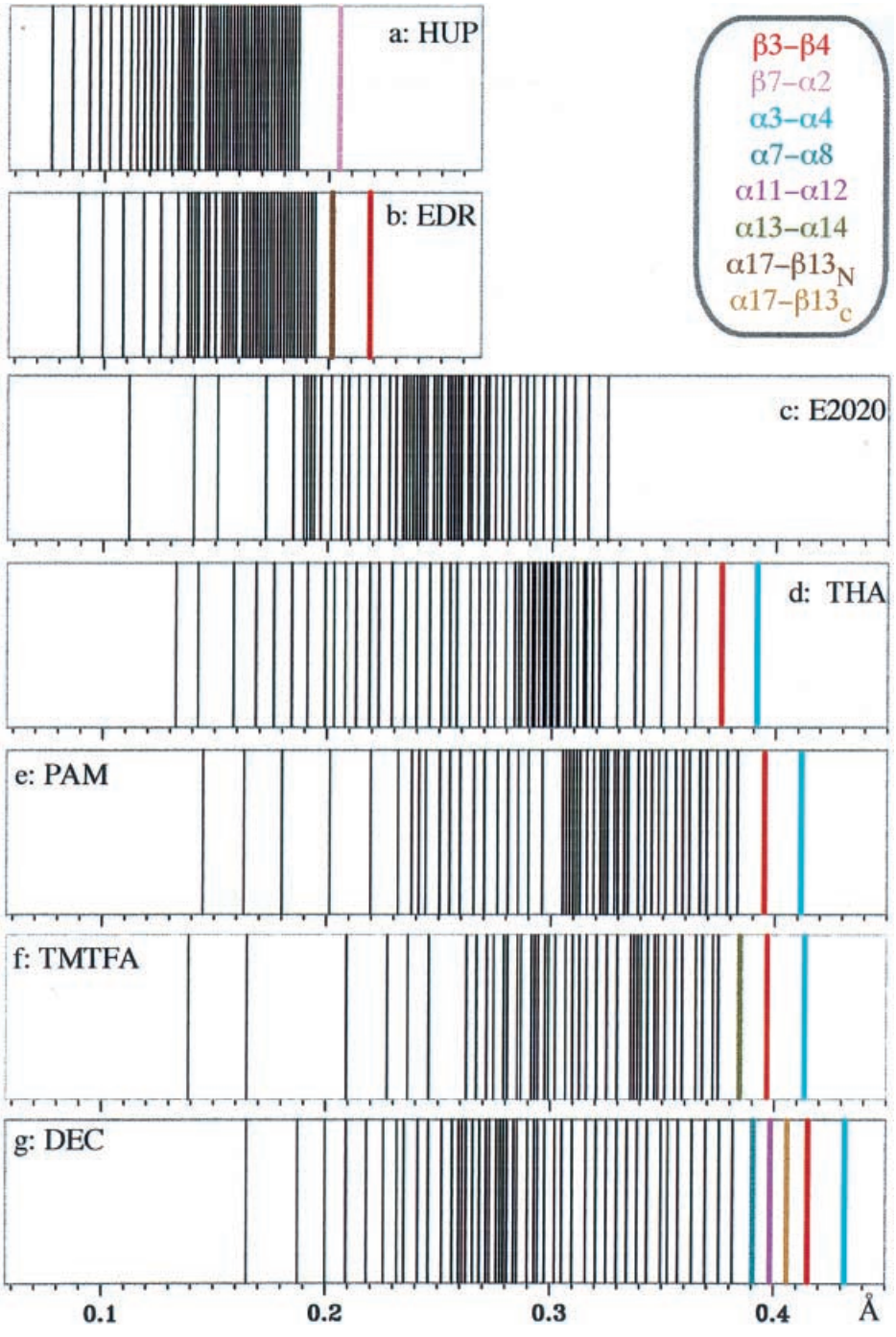

Fig. 2a–g. 1D representations of the jump-minimizing path derived from the multiple-linkage hierarchic clustering tree for the various TcAChE complexes, by the procedure of Ref. [17]. The figure shows the order in which individual secondary structures and loops, represented by *vertical lines*, are assembled along the jump-minimizing path, as a function of the root mean square deviation (*rmsd*) value of each assembly step, given on the abscissa. The segments which display sizable rmsd jumps upon their addition to the set of superimposed atoms define the major movers. They are added during the later steps of the path (*right-hand side* of the diagrams) and are highlighted in *colour*. All other segments are displayed in *black*

spanning residues 60–95, which a number of studies have linked to ligand traffic and binding [20]. Detailed analysis of the contacts made between neighbouring TcAChE molecules in the 2ACE crystal structure (data not shown) reveals that this loop is involved in such contacts. This suggests that the conformation of this loop in the crystal may differ from its solution conformation and probably that its flexibility in the crystal is also more restricted.

3.1.3.5 Links between the identified distortions or displacements in the 2.8-Å resolution complexes and ligand binding. Taking into account all these considerations, the main issue that needs to be addressed is the link between the identified deformations and ligand binding. This is not straightforward, not so much because the deformations are small and localized – we have shown indeed that our analysis correctly identifies such movements in HUP – but because the complexes in question are determined at 2.8-Å resolution and therefore represent less reliable models than those of the more recent structures, determined at 2.4–2.5-Å resolution. It is quite likely that a subset of the structural differences identified by our analysis may be related to model imprecision

rather than to ligand binding. In order to distinguish between these two possibilities, the displacements identified by our automatic procedure are analysed further with the aid of additional information. This information is obtained from visual inspection of the molecular models, analysis of the atomic contacts made between the enzyme and the ligand in each complex, and examination of the positions and interactions of water molecules in and near the active-site region.

Of the movers identified in the DEC complex, the structural changes of loops α9-α10 and α11-α12 are most likely due to ligand binding. These loops, which span residues 277–304 and residues 334–348, respectively, make contacts with the bound DEC via residues Trp_{279} and Tyr_{334}, as seen from the values of the enzyme–ligand contact areas listed in Table 4. On the other hand, in the native enzyme the 279–291 loop, an important constituent of the peripheral anionic site [11, 21] located in the first structural domain of AChE (Fig. 3), makes multiple contacts with the second domain across the active-site gorge [19]. The rmsd values of 0.45 Å for α9-α10 and 0.54 Å for α11-α12 indicate that observed displacements of these loops are most probably due to above-average local deformations. To further investigate the nature of these deformations, we applied the SoFi procedure using a smaller segment size of five residues. This allowed us to identify the specific portions in each loop which displayed the largest deformation. These turned out to be centred around residues Glu_{299} and Lys_{341}, respectively. Inspection of the DEC–TcAChE structure shows that the segment Gly_{298}-Glu_{299} belongs to a region with a high-temperature factor making the changes in the hydrogen-bonding pattern of Glu_{299} hard to interpret, though this residue makes a salt bridge with Arg_{47} in the native structure. Moreover, since Glu_{299} is located very far from the DEC ligand (Fig. 3), these movements are hard to rationalize. On the other hand, we see that Lys_{341} makes a hydrogen bond with a water molecule in both the native and complexed structures, while losing a strong hydrogen bond with Asp_{342} upon DEC binding. These changes seem to be accompanied by significant alterations in the side-chain conformation of these residues. Interestingly, Lys_{341} interacts with Phe_{75} and Phe_{78}, which are part of the ω loop and are both located in the first domain. It must be noted that another residue of this loop, Tyr_{70}, makes direct strong contacts with the ligand (Table 4), which are absent in the THA, PAM and TMTFA complexes, because unlike DEC they do not span the peripheral anionic site. The segment of the ω loop from Tyr_{70} to Trp_{84} makes contact with Tyr_{334}, Ser_{340} and Lys_{341}. Tyr_{70} is located near Asp_{72}, a residue that is involved in stabilizing ligands in the secondary anionic site, at the top of the active-site gorge, near Trp_{279} [3].

The relation to ligand binding of the other movers identified in this complex is more difficult to establish. The β3-β4 loop undergoes significant local deformation (Tables 2, 3) and is a mover in all other complexes, except HUP and E2020 (Fig. 2). However, as discussed in the previous section, its deformation is most likely related to model imprecisions rather then to ligand binding. This suggestion is further confirmed by the fact that the same loop is singled out as a mover relative to the free enzyme (2ACE), also in the 2.8-Å resolution TcAChE–FAS complex (discussed later), where the ligand (the FAS protein) does not enter the enzyme gorge, but is bound to the protein surface.

Similar conclusions can be drawn for the deformations in the segments between α17 and β13. As already mentioned, these segments flank missing residues in the models of both the free and the complexed enzymes.

The origins of the displacements, or deformations in remaining "movers", are more difficult to evaluate. In DEC, these segments comprise α3-α4, helix α8, the adjacent loop α7-α8 and α13-α14. A subset of these segments appears as movers in the remaining complexes of Fig. 2d, e, f and g. The fact that none of the corresponding segments makes direct contact with the bound inhibitors makes it unlikely, however, that the bound molecules affect their conformation, although the possibility of indirect effects can, in principle, not be ruled out. Indeed, an extensive contact area (20–30 $Å^2$) is formed between residues 251–277, 251–280 and 252–277, which belong to α7-α8 and the top of segment α9-α10 (Fig. 3), near Trp_{279}. Also, the bottom of segment α9-α10, near residue 299, interacts with α3-α4. Contacts between residues 156–292, 157–295, 159–297, 166–295, 167–295 and 167–300 are also detected, and the value of the interface areas between the contacting residues are altered by the nature of the bound ligand. These effects could be due to a small rearrangement of the structure upon binding, but we cannot exclude the fact that these changes may be due to the poorer quality of the model in these specific regions.

To gain further insight into the possible causes for the deformations of these segments, we analysed in detail the atomic models in the corresponding region, with particular focus on the positions of the crystallographically determined water positions. Figure 4 displays nine panels showing the water positions in the region where segments α3-α4, α9-α10 and α7 meet each other in the 3D structure of the free AChE and in eight of the complexes analysed. In 2ACE five crystallographic water molecules, numbered 601, 614, 626, 675 and 698, are located in this region and form a network of hydrogen bonds with the enzyme structure. Water molecule 614 makes a hydrogen bond with residues of the segment α9-α10, water molecules 601 and 675 bridge residues in α7 to those of the α3-α4 loop, whereas water molecules 626 seems to bridge the segments α3-α4 and α9-α10. Water 698 appears to stabilize the structure of the α3-α4 loop. Not too surprisingly, a virtually identical arrangement is observed in the three higher-resolution complexes, 1VOT, 2ACK and 1EVE, in which the conformation of α3-α4 is similar to that in 2ACE (Table 2).

This is not the case for the other 2.8-Å complexes displayed in Fig. 4. Interestingly, we see that these models tend to have fewer water molecules than 2ACE in the same region. The complex with PAM and that with THA (1ACJ) also retain only two of the four water positions in this region; the remaining positions correspond to water molecules 601 and 614. In these two structures the deformations in the α3-α4 loop are larger and range between 0.75 and 0.76 Å rmsd. The largest deformations of the α3-α4 loop are encountered in the complex with TMTFA,

Table 4. Contacts made by the ligands with residues of the proteins. These interactions are evaluated from the contact areas between atoms computed using the program Survol [22]. The Protein Data Bank code of the protein, the name of its main ligand and, if applicable, the counterion are indicated in the top row. The leftmost column lists all the TcAChE residues making interactions with at least one of the ligands analysed. The others columns list the contact areas (in square angstroms). Values of the contact area of 20 Å or greater are in *bold*. The values in italic correspond to those with the counterion

	2ACE ACH	1VOT HUP	2ACK EDR	1EVE E2020; NAG	1ACL DEC	1ACJ THA	PAM PAM; SUL	1AMN TMTFA; SO4
59				**36.0**				
61				*13.4*				
62				*14.0*				
70				16.6	17.3			
72				8.7	1.2	3.5		
80						0.9		
81						1.9		
84	**24.6**	**49.5**	**32.5**	**35.3**	**28.8**	**50.4**	**37.0**	**25.2**
116		**1.8**						
117		7.3	3.1	5.0	3.7	4.0	10.4	2.8
118	16.7	**23.3**	**20.1**	12.0	9.4	11.8	6.6; *10.1*	17.2
119	9.6	4.4	6.5				*9.6*	18.0
121		13.6	11.5	**23.2**	**24.2**		***20.3***	11.6; *9.0*
122		10.4	4.1			1.8	*4.4*	
123		11.3					2.0	
127		4.1					0.1	
130		11.7	2.5	3.7	4.5	3.1	10.4	1.5
199	7.3	8.6	7.8	10.0	8.9	9.1	11.2	10.5
200	16.4	4.8	10.6	1.7	5.8	3.6	0.1; *1.4*	18.1
201	1.9							6.7
233	2.9		0.6					15.5
279				**41.2**	**23.6**			*5.6*
282				7.6				
286				8.2				*3.5*
287				0.5				*9.2*
288	4.8		2.8	5.0				13.8; *18.7*
289				5.6				4.0; *11.1*
290	4.2	4.2	5.4	10.6	4.9		*8.3*	10.3; *11.0*
330	15.8	**29.0**	**21.5**	**31.4**	**33.0**	**35.5**	18.2; *8.7*	12.3; *3.2*
331	7.8	10.5	10.8	**27.3**	19.1		0.1; *14.4*	13.9; *30.6*
334				**33.3**	36.7	5.0		13.8; *15.1*
335								*10.1*
415				*5.1*				
416				***46.9***				
417				*2.9*				
429				*3.4*				
431				*0.8*				
432						11.3		
436						1.1		
439		0.1				5.1	0.9	
440	**23.8**	**20.8**	**26.0**	14.8	13.8	16.9	**21.4**; *9.1*	**25.8**
441	4.4	4.2	4.8	2.5	3.9	4.9	3.8	0.5
442		2.5	0.9			6.1	0.6	
444			0.4		0.8	0.4		0.1
455				*7.1*				
456				*16.8*				
457				***35.5***				
494				*11.7*				
533				***55.3***				

which has lost all but water molecule 601 in this region, and in the complex with DEC, which has no water position in this region. These observations suggest a link between the size of the observed deformations of segment α3-α4 and the interpretation of the electron density map in the nearby region, which involves positioning of water molecules. It is thus most likely that these deformations as well as those observed in the neighbouring fragments α8 and α7-α8, arise from model imprecisions rather than from ligand binding. The fact that the deformation of α3-α4, and for that matter those of the other segments, is not detected in the 2.4–2.5-Å resolution complexes (Fig. 2a, b, c) confirms this hypothesis.

Problems with the model could also be at the origin of the deformations of the α13-α14 loop, located at the top of the enzyme active-site gorge in the complexes with

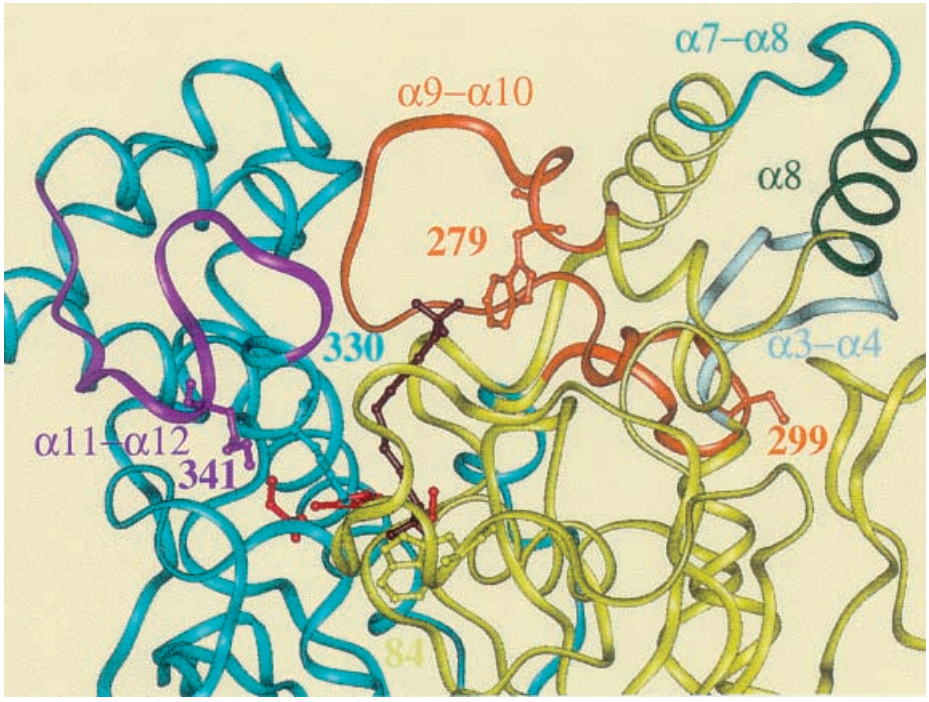

Fig. 3. Ribbon diagram of the decamethonium (*DEC*) –TcAChE (PDB code 1ACL) arround the active site. The first domain of TcAChE is in *green*, while the second one is in *cyan*. The loops α3-α4, α7-α8, α8, α9-α10 and α11-α12, which undergo local deformations relative to the free enzyme, are highlighted in *different colors*. Side chains of the catalytic triad are shown in *red*. Key residues (Trp_{84}, Trp_{279}, Phe_{330}), Glu_{299} and Lys_{341} have also their side chains displayed in *stick form*. The DEC ligand is represented in *brown*. This figure was generated using the software InsightII

DEC and TMTFA. Inspection of the structure in this region reveals that the first two residues of α14 (384, 385) are in contact with residue 346, which belongs to the α11-α12 loop. This latter loop makes direct interactions with the DEC and TMTFA ligands. Indirect effects due to ligand binding in this complex can therefore not be ruled out.

In summary, our analysis indicates that DEC binding induces structural changes in two regions, loop segments α9-α10 and α11-α12 both localized at the top of the active-site gorge and making direct contact with the DEC ligand. As to other weaker movers identified in the DEC structure relative to the native 2ACE (segments α7-α8, α8, α3-α4 and α13-α14), inspection of the structure and analysis of the contacts with ligand and water suggests that the corresponding deformations are probably due to imprecisions of the model of the DEC–TcAChE complex, although indirect effects induced by the presence of the ligands cannot be ruled out. Ligand-induced structural changes do not seem to occur in the complexes with the smaller ligands, PAM, THA and TMTFA, which are confined to the bottom of the gorge.

3.2 Structural changes induced by FAS binding

Having applied our automatic MLC procedure to investigate the structural deformations of TcAChE in the complexes with small quaternary ammonium ligands, it seemed worthwhile to extend our analysis to the complex of TcAChE with the a small protein inhibitor, the snake venom toxin FAS-II, despite the fact that this complex was solved only to 3.0-Å resolution (PDB code 1FSS) [14]. The crystallographic study has revealed that the FAS molecule binds at the top of the active-site gorge, at a location overlapping the peripheral anionic site, suggesting that its inhibitory action may result from steric occlusion of the enzyme active site.

The optimal global structure alignment of the TcAChE–FAS complex and the free enzyme, obtained with the MLC procedure, has an rmsd of 0.43 Å when only the secondary structures are superimposed, increasing marginally (0.51 Å) when the loops are also aligned. These rmsd values are higher than those obtained for the complexes with the quaternary ammonium ligands, indicating that the TcAChE–FAS structure differs more from that of the free enzyme than those structures.

As for the small-ligand complexes, individual secondary structures in TcAChE–FAS display negligible local structural deformations (Table 3), but a number of loops undergo significant local conformational changes. The largest local deformation (1.09 Å rms) occurs in β3-β4, also the most deformed loop in the small-ligand complexes. The next largest local distortion (0.78 Å rms) is in the segment between β11 and α12. This segment comprises the stretch assigned as helical (α11) by DSSP [18] in the free enzyme, but as a turn region in the FAS complex. α9-α10, the third loop to undergo local changes, is less deformed than the first two, but its conformation changes more relative to the free enzyme (0.62 Å) than in the DEC complex, which is the only small-molecule complex where this loop also changes.

Four additional loops are slightly distorted: α3-α4 and α17-$\beta13_N$, which also display changes in the other ligand complexes, and β13-β14 and β5-α1, which do not. Interestingly, the β5-α1 loop is part of the ω loop, which in the FAS complex does not participate in crystal contacts. The structural differences detected in these loops may thus result either from differences in the crystal environment in the two compared structures or from ligand binding.

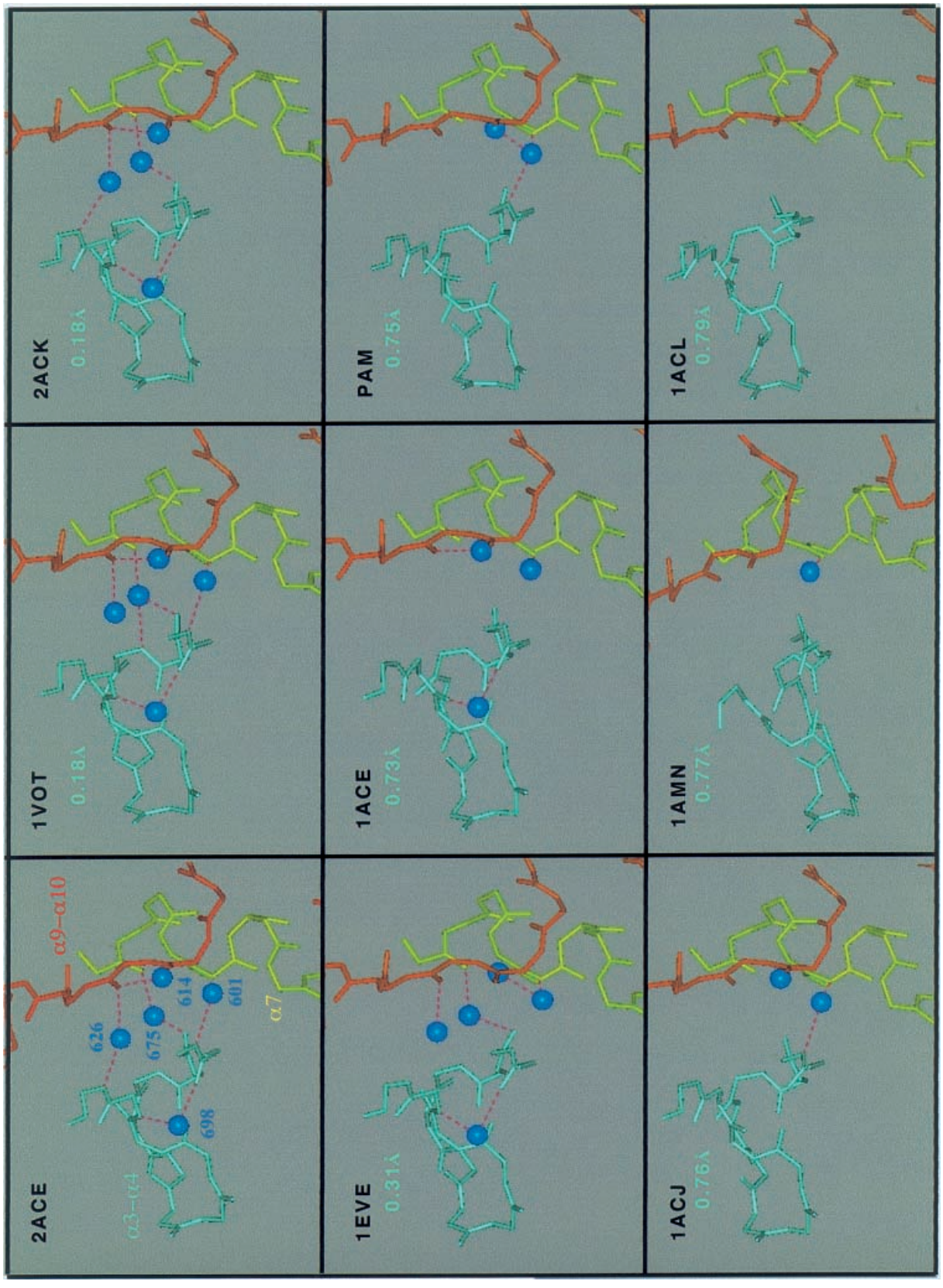

Fig. 4. Water positions in the region where the segments α3-α4, α9-α10 and α7 meet each other in the 3D structure of the free TcAChE. The crystallographic water molecules are represented by *blue balls*. The numbering is that in the 2ACE structure. Hydrogen bonds are in *red dashed lines*. The backbone rmsd of loop α3-α4 is indicated in *light cyan* for the seven complexed structures and the ''old'' free enzyme structure (1ACL),which contains the DEC ligand

The static core identified from the jump-minimizing path comprises 29 of the 31 secondary structure elements of TcAChE (Fig. 5b). Inspection of this path, shows that the two remaining helices, α12 and α19, are displaced relative to this core. Since the conformations of these helices are very similar in the complexed and free enzymes (Table 3), the displacements detected represent rigid-body movements of these helices relative to the core. Detailed inspection of Fig. 5b. reveals furthermore that helices α13 and α9, considered to be part of the static core by our criteria (see Sect. 2), display larger rms jumps than other segments in this core, indicating that they too display small rigid-body movements.

Loop movements were identified from the jump-minimizing path derived from the comparisons that take into account loop segments as well. This path, illustrated in Fig. 5c, reveals that three loops undergo significant displacements relative to the static core. The major mover is the segment β11-α12, which include the stretch assigned as helix (α11) in the free enzyme. Adding it to the rest of the protein produced an rms jump (0.48–0.52 Å), which is quite large according to our criteria. Five other loops display smaller relative displacements, which are mainly due to their local distortions (Table 3). These are α9-α10, β3-β4, α17-$\beta13_N$, β5-α1 and α3-α4. As in the case of the quaternary ammonium ligand complexes, only a subset of the detected structural differences is probably related to FAS binding.

The differences in the loops β3-β4 and α17-$\beta13_N$ are most likely not a consequence of toxin binding, but are due to structural imprecisions, as discussed in our analysis of the other complexes. The same goes for the

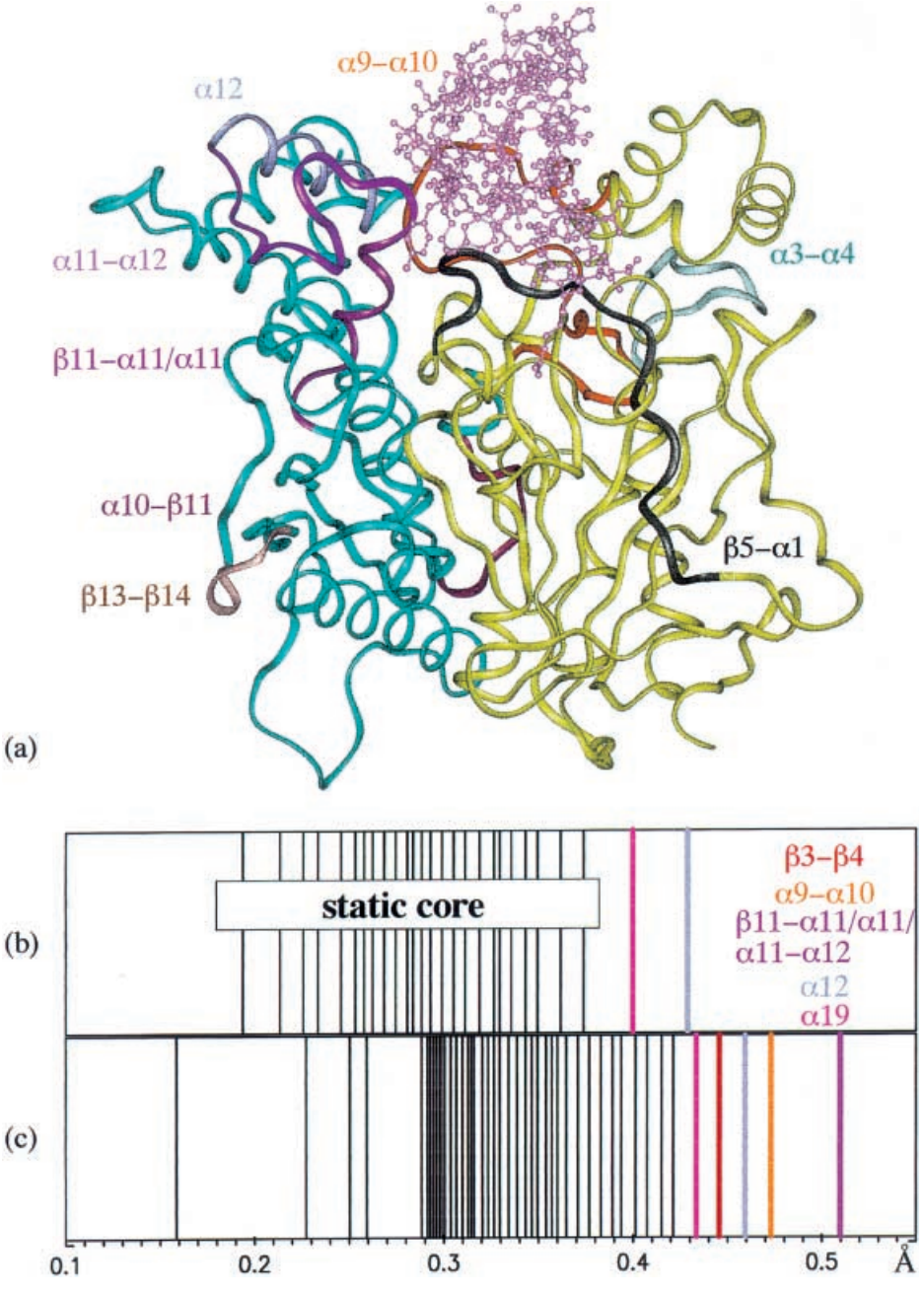

Fig. 5a–c. Conformational change in fasciculin (*FAS*)–TcAChE. **a** Ribbon drawing of the TcAChE ligated to FAS. The toxin FAS is shown in *pink*, while the enzyme is in *green*. The TcAChE segments that undergo small conformational changes relative to the free enzyme are highlighted by *others colors*. **b** 1D representation of the jump-minimizing path along the clustering trees obtained by aligning only the secondary structures. Those which make up the static core are framed. (See legend of Fig. 2 for details) **c** 1D representation of the jump-minimizing path computed from the MLC alignment which consider all segments. (See the legend of Fig. 2 for details)

changes in α19, as this helix is located near the protein C terminus, a good distance from the toxin binding site.

Inspection of the TcAChE–FAS crystal structure shows that the toxin interacts with three main regions of AChE comprising residues 68–90, 272–289 and 334–358 [14] (Fig. 5a). Two of these regions clearly overlap with major movers identified in the jump-minimizing paths of Fig. 5c, namely segments α9/α9-α10 (271–304) and β11-α12/α12 (319–348). In both segments the helices (α9 and α12) move as rigid bodies, while their flanking loops (β11-α11, α11-α12 and α9-α10) undergo local distortions. The third contact region of FAS involves the ω loop, which overlaps with the β5-α1 loop (residues 60–78). The latter undergoes mainly local distortions (Table 3), relative to the conformation in the free enzyme.

Our automatic conformational change analysis and model inspection thus provide a very similar description of the backbone movements undergone by the enzyme FAS binding as those obtained by manual analyses performed by crystallographers.

4 Concluding remarks

In this study we applied a completely automatic procedure to investigate the changes in the backbone structure in eight complexes of TcAChE with various small-molecule ligands and in the complex with the protein toxin FAS. This procedure confirmed that the enzyme backbone undergoes very small structural changes upon ligand binding in all the complexes analysed, with values of the rms backbone deformations not exceeding 0.41 Å for the complexes and 0.52 Å for the FAS–TcAChE complex. In addition, it identified a few segments in each complex with the small molecules, which undergo above-average local deformations. Since five of the complexes considered are relatively imprecise models (2.8-Å resolution, with limited refinement), the results of the automatic procedure were complemented by model inspection and by analysis of the atomic contacts made by the enzyme with the ligand and water molecules. This was done in an attempt to discriminate between structural changes arising from model imprecision and those caused by ligand binding.

We found that except for the peptide flip, HUP–TcAChE, readily detected by our automatic procedure, the backbones of other complexes with quaternary ammonium ligand display negligible changes relative to that of the free enzyme. Another exception was the complex with DEC, where several loops displayed above-average deformations, but only two, the loop comprising residues 277–304 and that comprising residues 334–348, seem to be caused by ligand binding. Interestingly, our analysis detected no significant movements in the ω loop (residues 61–95). We suggest that this is due to the fact that this loop is involved in crystal contacts and that, therefore, the conformation of this loop in the crystal structures examined is probably different from its solution conformation. This conclusion seems to be supported by our findings that the conformation of this loop is somewhat different in FAS–TcAChE, which crystallizes in a different from, where this loop is not engaged in crystal contacts.

Our study therefore provides further support to the findings that the binding of small ligands to the active site of AChE can occur without any significant backbone adjustments and is probably enabled by small side-chain movements and transient backbone adjustments. Only ligands that bind to the top of the gorge, at or near the peripheral ionic site, seem to cause some backbone changes localized in the two previously mentioned loops. The ligands in this study which seems to cause changes in this region are the bisquaternary ammonium ligand DEC, which binds to both the active and the peripheral sites, and the protein inhibitor FAS, which binds to the top of the gorge, seemingly blocking its entrance.

References

1. Barnard EA (1974) In: Hubbard JI (ed) The peripheral nervous system.pp Plenum, New York, pp 201–224
2. Hallak M, Giacobini E (1989) Neuropharmacology 28: 199–206
3. Sussman JL, Silman I (1992) Curr Opin Struct Biol 2: 721–729
4. Sussman JL, Harel M, Frolow F, Oefner C, Goldman A, Toker L, Silman I (1991) Science 253: 872–879
5. Bourne Y, Taylor P, Kanter JR, Bougis PE, Marchot P (1998) In: Doctor BP, Quinn DM, Rotundo RL, Taylor P (eds) Structure and function of cholinesterases and related proteins. Plenum, New York, pp 315–322
6. Kryger G, et al (1998) In: Doctor BP, Quinn DM, Rotundo RL, Taylor P (eds) Structure and function of cholinesterases and related proteins. Plenum, New York, pp 323–326
7. Quinn DM (1987) Chem Rev 87: 955–975
8. Radic Z, Reiner E, Taylor P (1991) Mol Pharmacol 39: 98–104
9. Taylor P, Radic Z (1994) Annu Rev Pharmacol Toxicol 34: 281–403
10. Harel M, Quinn DM, Nair HK, Silman I, Sussman JL (1996) J Am Chem Soc 118: 2340–2346
11. Harel M, Shalk I, Ehret-Sabatier L, Bouet L, Goeldner M, Hirth C, Axelsen PH, Silman I, Sussman JL (1993) Proc Natl Acad Sci USA 90: 9031–9035
12. Raves ML, Harel M, Pang YP, Silman I, Kozikowski AP, Sussman JL (1997) Nat Struct Biol 4: 57–63
13. Kryger G, Silman I, Sussman IL (1999) Structure 7: 297–307
14. Harel M, Kleywegt GJ, Ravelli RBG, Silman I, Sussman JL (1995) Structure 3: 1355–1366
15. Radic Z, Gibney G, Kawamoto S, MacPhee-Quingley K, Boungiorno C, Taylor P (1992) Biochemistry 31: 9760–9767
16. Boutonnet N, Rooman M, Wodak S (1995) J Mol Biol 253: 633–647
17. Boutonnet N, Rooman M, Ochagavia ME, Richelle J, Wodak S (1995) Protein Eng 8: 647–662
18. Kabsch W, Sander C (1983) Biopolymers 22: 2577–2637
19. Morel N, Bon S, Greenblatt HM, Van Belle D, Wodak S, Sussman JL, Massoulie J, Silman I (1999) Mol Pharmacol 55: 982–992
20. Weise C, Kreienkamp HJ, Raba R, Pedak A, Aaviksaar A, Hucho F (1990) EMBO J 9: 3885–3888
21. Bourne Y, Taylor P, Marchot P (1995) Cell 83: 503–512
22. Alard P (1992) PhD thesis. Free University of Brussels, Brussels, Belgium, p 120